

Supporting information

Axial modulation of Fe sites realizing high-performance oxygen reduction reaction of FeN₄ catalysts

Yu Zhang,^[a,b] Caixia Li,^{*[a,c]} Jin Li,^[a,b] Xiaoni Liu,^[a,c] Guangjiu Li,^[b] Bin Li^[a] and Lei Wang^{*[a, b, c]}

^a State Key Laboratory Base of Eco-Chemical Engineering, International Science and Technology Cooperation Base of Eco-chemical Engineering and Green Manufacturing, Qingdao University of Science and Technology, Qingdao 266042, P. R. China.

^b College of Chemistry and Molecular Engineering, Qingdao University of Science and Technology, Qingdao 266042, China.

^c Shandong Engineering Research Center for Marine Environment Corrosion and Safety Protection, College of Environment and Safety Engineering, Qingdao University of Science and Technology, Qingdao, 266042, P. R. China.

****Corresponding Author:***

*E-mail: licaixia91@126.com (C. Li),

*E-mail: inorchemwl@126.com (L. Wang)

Table of Contents

1. Chemicals and Reagents
2. Apparatus and Measurements
3. Oxygen Reduction Reaction Measurements
4. Construction of Zn-Air Batteries
5. Supporting Figures and Tables

1. Chemicals and Reagents

Chemicals	Purity	Company
Aluminum nitrate nonahydrate ($\text{Al}(\text{NO}_3)_3 \cdot 9\text{H}_2\text{O}$)	99.9%	Shanghai Aladdin Bio-Chem Technology Co., LTD
Iron(III) nitrate nonahydrate ($\text{Fe}(\text{NO}_3)_3 \cdot 9\text{H}_2\text{O}$)	98.5%	Sinopharm Chemical ReagentCo., Ltd
1,4-Naphthalenedicarboxylic acid	95%	Shanghai Aladdin Bio-Chem Technology Co., LTD
Hydrofluoric acid (HF)	$\geq 40\%$	Sinopharm Chemical ReagentCo., Ltd
Zinc acetate	99%	Sinopharm Chemical ReagentCo., Ltd
Potassium hydroxide (KOH)	$\geq 85\%$	Sinopharm Chemical ReagentCo., Ltd
Nafion	5 wt. %	Sigma Aldrich
20% Pt/C powders (HiSPEC 3000)	20% Pt	Alfa Aesar

De-ionized (DI) water with a specific resistance of $>18.2 \text{ M}\Omega \cdot \text{cm}$. All chemicals were purchased and used without further purification.

2. Apparatus and Measurements

XRD measurements were conducted on a X'Pert PRO MPD instrument. Raman spectra were tested by Invia spectrometer with an excitation laser wavelength of 532 nm. XPS was carried out using VG ESCALABMK II with Al $K\alpha$ radiation (1486.6 eV) photon source. N_2 adsorption and desorption analysis was performed by Micrometrics ASAP 2020 at 77 K. Pore size distributions of samples were calculated by using the non-localized density functional theory (NLDFT) method and mesopore volumes were evaluated by Barrett, Joyner and Halenda (BJH) method. Morphologies of samples were analyzed by the scanning electron microscope (Hitachi S-8200). The transmission electron microscopic (TEM) and high-annular dark-field scanning TEM (HAADF-STEM) images were collected on JEM-ARM200F and JEM-F200. The ICP and elemental analyses were performed by Agilent 730 and Elementar UNICUBE, for ICP and elemental analysis, respectively. Fe K-edge analysis was performed with Si(111) crystal monochromators at the BL11B beamlines at the Shanghai Synchrotron

Radiation Facility (SSRF) (Shanghai, China). Before the analysis at the beamline, samples were pressed into thin sheets with 1 cm in diameter and sealed using Kapton tape film. The XAFS spectra were recorded at room temperature using a 4-channel Silicon Drift Detector (SDD) Bruker 5040. Fe K-edge extended X-ray absorption fine structure (EXAFS) spectra were recorded in transmission mode. Negligible changes in the line-shape and peak position of Fe K-edge XANES spectra were observed between two scans taken for a specific sample. The XAFS spectra of these standard samples (FePC, Fe₂O₃, and Fe₃O₄) were recorded in transmission mode. The spectra were processed and analyzed by the software codes Athena and Artemis.

3. Oxygen Reduction Reaction Measurements

The ORR electrochemical measurements were performed on a CHI 760E electrochemical workstation. ORR electrochemical measurements were tested in a conventional three-electrode system at room temperature. A platinum sheet and an Ag/AgCl electrode in saturated aqueous potassium chloride solution were used as counter and reference electrodes, respectively. Different catalysts were dispersed in a mixture of deionized water, isopropanol, and 5 % Nafion solution in the volume ratio of (v:v:v = 5:19:1) and treated by sonication for 45 min to obtain a homogeneous catalyst ink with a concentration of 5 mg mL⁻¹. A glassy carbon rotating disk electrode (RDE, 5 mm diameter, 0.196 cm² geometric surface area) loaded with catalyst was used as a working electrode. In the ORR test, the loading amount of each catalyst was 0.255 mg cm⁻². All potentials in this study referred to the reversible hydrogen electrode (RHE, $E_{\text{RHE}} = E_{\text{Ag/AgCl}} + 0.0592 \text{ pH} + 0.1976 \text{ V}$).

In the ORR activity test, LSV curves were recorded in O₂-saturated 0.1 M potassium hydroxide with a scan rate of 10 mV s⁻¹ and a speed of 1600 rpm. the Tafel slope (b) was obtained by fitting the linear part according to the following equation:

$$\eta = b \log(j) + a$$

where η and j are the overpotential (V) and current density (mA cm⁻²), respectively.

The electron transfer number (n) in the ORR test is determined by the K-L equation as

follows:

$$\frac{1}{j} = \frac{1}{j_k} + \frac{1}{j_l} = \frac{1}{j_k} + \frac{1}{B\omega^{1/2}}$$

$$B = 0.2nFD_0^{2/3}\nu^{-1/6}C_0$$

where j is the current density, j_k is the kinetic current density, j_l is the limiting current density, and ω is the angular speed of rotation of the electrode (rpm), n is the number of electron transfers, F is Faraday's constant ($F = 96485 \text{ C mol}^{-1}$), D_0 is the O_2 diffusion coefficient ($1.9 \times 10^{-5} \text{ cm}^2 \text{ s}^{-1}$) in a 0.1 M KOH electrolyte, ν is the kinematic viscosity of the electrolyte ($0.01 \text{ cm}^2 \text{ s}^{-1}$), and C_0 is the volume concentration of O_2 ($1.2 \times 10^{-6} \text{ mol cm}^{-3}$)

For RRDE measurement, the working electrodes were prepared by the same process as RDE. The rotation rate was 1600 rpm and ring potential was set at a constant value of 1.2 V vs RHE. The H_2O_2 % and electron transfer number were determined by the following equations:

$$\text{H}_2\text{O}_2\% = 200 \times \frac{I_r/N}{I_d + I_r/N}$$

$$n = 4 \times \frac{I_d}{I_d + I_r/N}$$

Where I_d is the disk current and I_r is the ring current, N is the current collection efficiency (0.37) of the Pt ring.

We have employed the VASP ^[1,2] to perform all the density functional theory (DFT) calculations within the generalized gradient approximation (GGA) using the Perdew-Burke-Ernzerhof (PBE) ^[3] formulation. We have chosen the projected augmented wave (PAW) potentials ^[4] to describe the ionic cores. Take valence electrons into account using a plane wave basis set with a kinetic energy cutoff of 450 eV. Partial occupancies of the Kohn-Sham orbitals were allowed using the Gaussian smearing method and a width of 0.05 eV. The electronic energy was considered self-consistent when the energy change was smaller than 10^{-5} eV. A geometry optimization was considered convergent when the energy change was smaller than 0.03 eV/Å. The Brillouin zone is sampled with $3 \times 3 \times 1$ Gamma kpoints ^[5]. The free energy on surface was calculated as follows: $\Delta G = E(\text{DFT}) + \Delta E(\text{ZPE}) - T\Delta S$, where $E(\text{DFT})$ is the total energy for the adsorption OOH^* , OH^* and O^* , $\Delta E(\text{ZPE})$ is the zero-point energy change and ΔS is the entropy

change.

4. Zn-Air batteries

For the zinc-air cell, a zinc plate with a thickness of 0.5 mm was used as the anode and a mixture of 6.0 M KOH and 0.2 M Zn(OAc)₂ was used as the electrolyte. For the air cathode, FeN₄S₁ (10 mg), carbon black (5 mg) and 5 % polytetrafluoroethylene (PTFE) were used. The polytetrafluoroethylene (PTFE) dispersion (20 μL) was first dispersed into isopropyl alcohol (1.0 mL) and dried at 60 °C. The resulting mixture and waterproof breathable film were then pressed onto the two surfaces of nickel foam under ultrasonic treatment. Pt/C as an air cathode was also fabricated as described above. About the performance test of Zn-air cell. We performed polarization curve tests on an electrochemical workstation (CHI 760E) and collected charge/discharge curves on a LANHE CT2001. The cycle tests were performed at a current density of 10 mA cm⁻² for 20 minutes per cycle, each cycle consisting of 10 minutes of charging and 10 minutes of discharging.

5. Supporting Figures and Tables

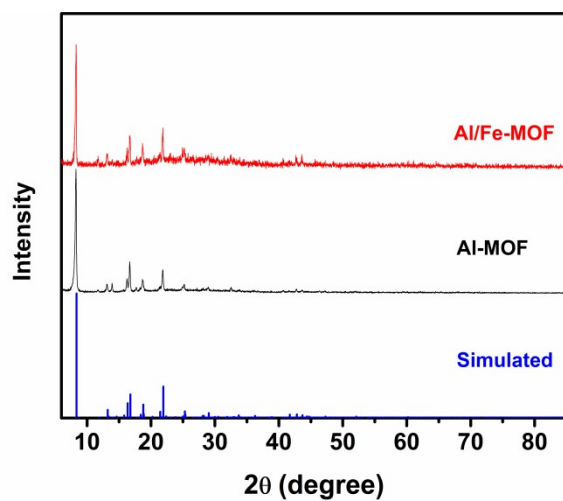


Figure S1. XRD patterns of Al-MOF, Al/Fe-MOF and Al-MOF (simulated).

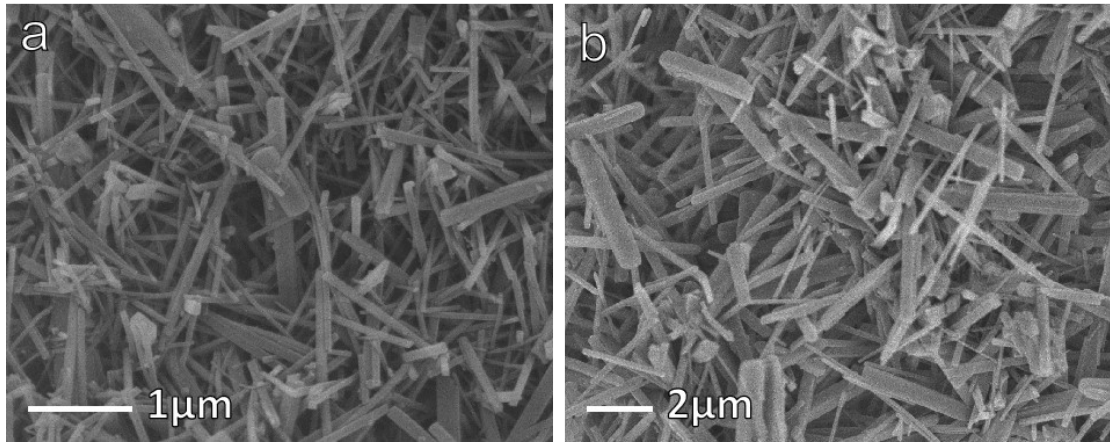


Figure S2. The SEM images of (a) Al-MOF and (b) Al/Fe-MOF.

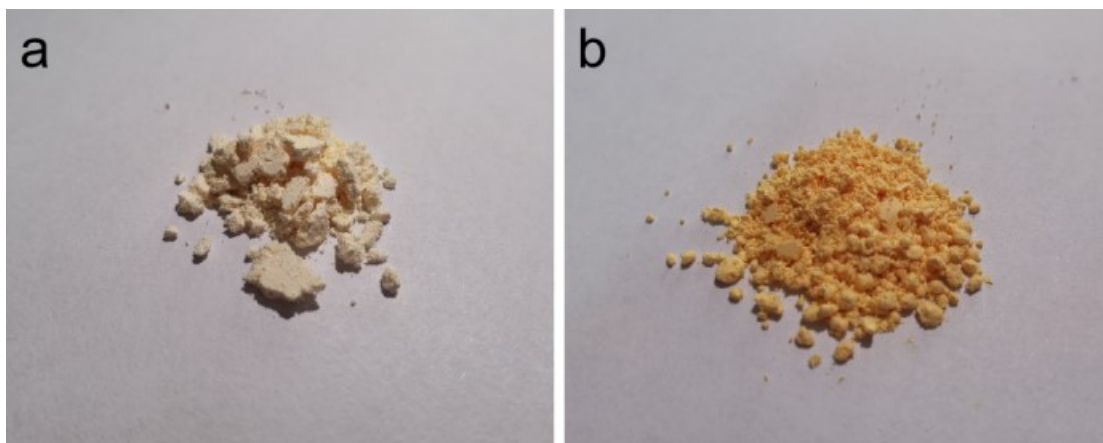


Figure S3. The photograph of (a) Al-MOF and (b) Al/Fe-MOF.

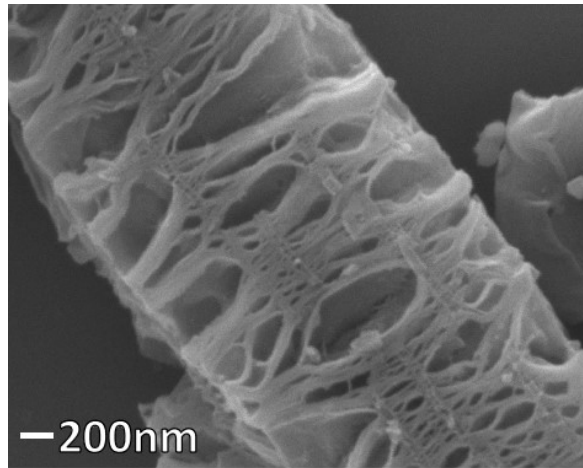


Figure S4. The SEM image of Fe-N₄S₁.

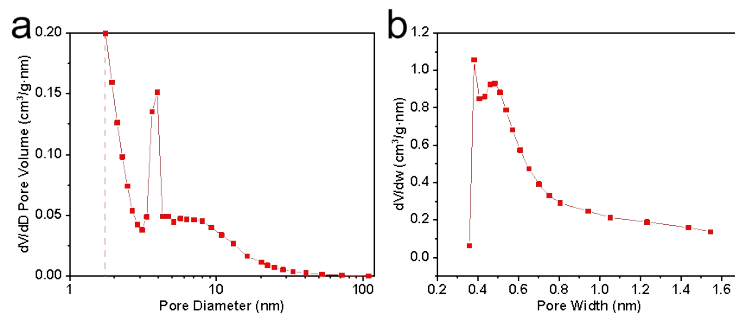


Figure S5. Pore size distribution of Fe-N₄S₁ sample.

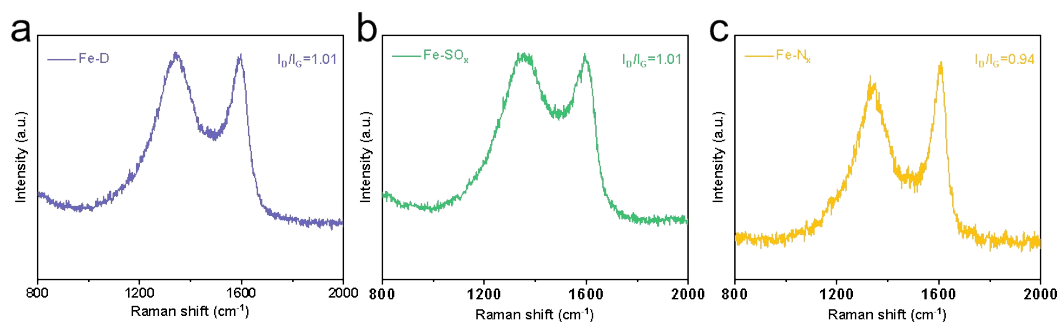


Figure S6. The Raman spectra of (a) Fe-D, (b) Fe-SO_x and (c) Fe-N_x.

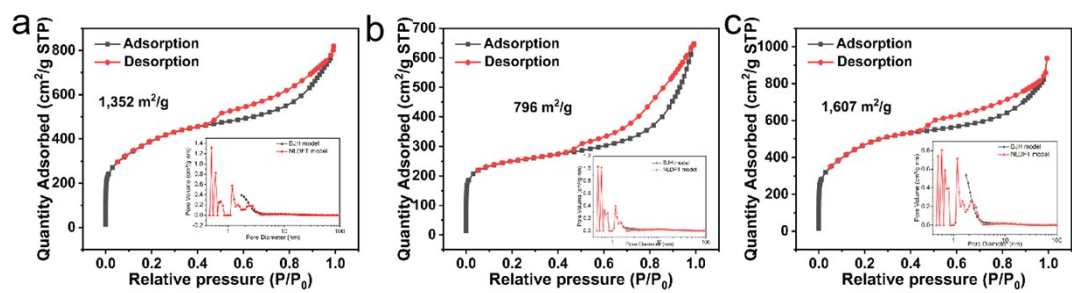


Figure S7. N_2 adsorption and desorption curves of (a) Fe-D, (b) Fe-SO_x, (c) Fe-N_x.

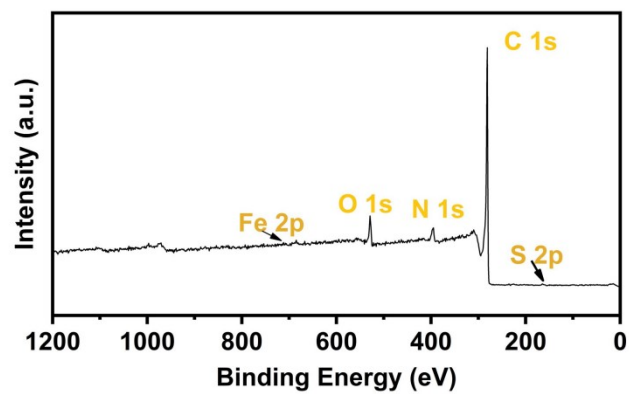


Figure S8. Full spectrum of XPS of Fe-N₄S₁ samples.

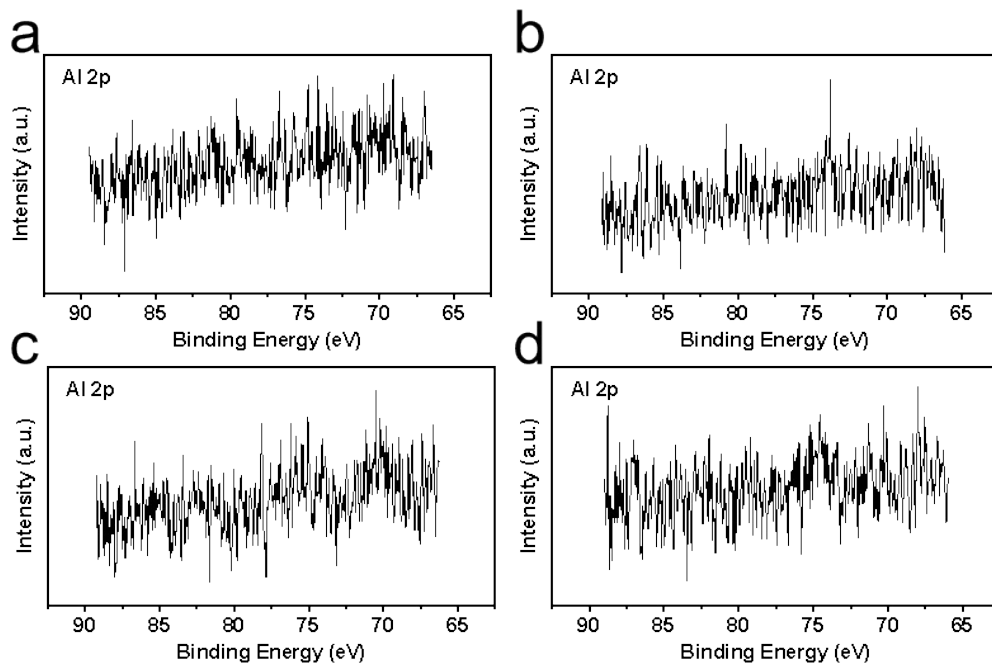


Figure S9. XPS curves of Al 2p for (a) Fe-D, (b) Fe-SO_x, (c) Fe-N_x and (d) Fe-N₄S₁.

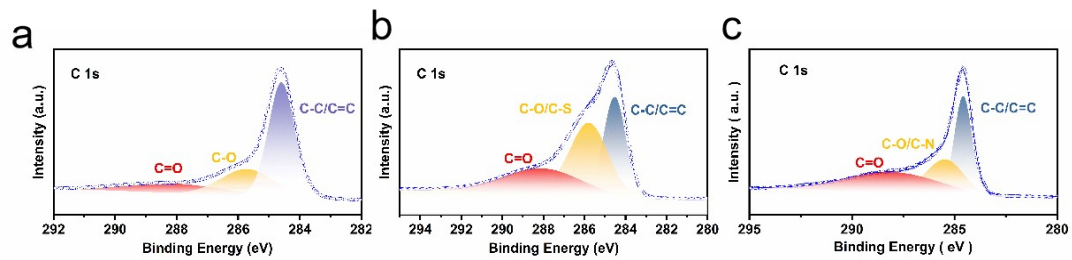


Figure S10. XPS curves of C 1s for (a) Fe-D, (b) Fe-SO_x and (c) Fe-N_x.

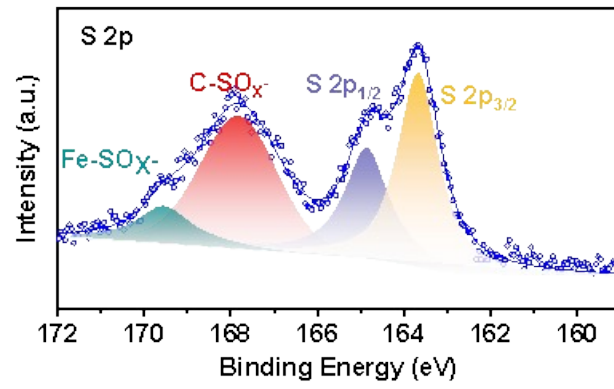


Figure S11. XPS curves of S 2p for Fe-SO_x.

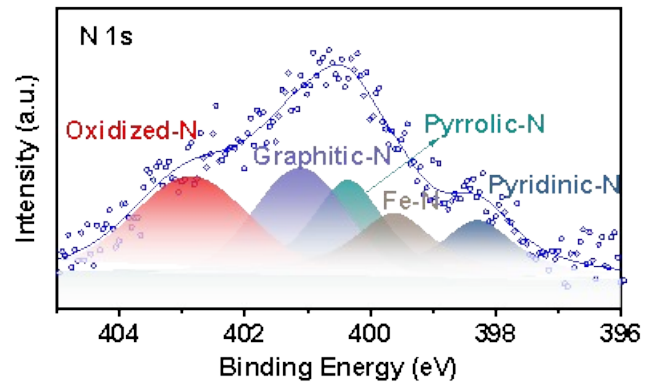


Figure S12. XPS curves of N 1s for Fe-N_x.

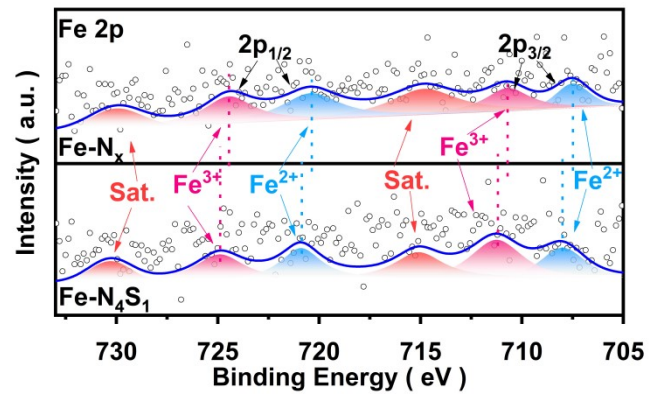


Figure 13. XPS curves of Fe 2p for Fe-N₄S₁ and Fe-N_x.

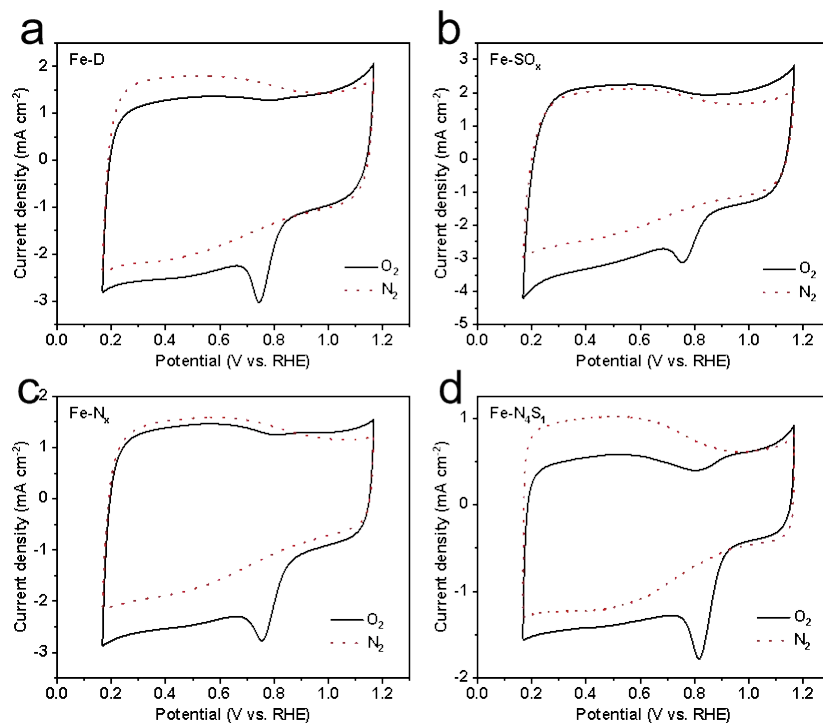


Figure S14. CV curves of Fe-N₄S₁ and comparison samples in O₂ and N₂-saturated 0.1 M KOH.

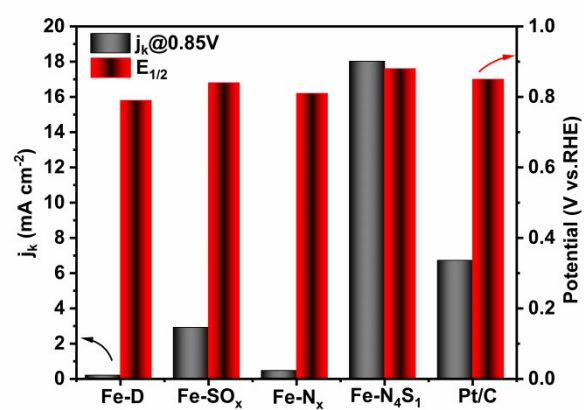


Figure S15. Kinetic current density ($j_k@0.85$ V) and $E_{1/2}$ of Fe-N₄S₁ and comparison samples.

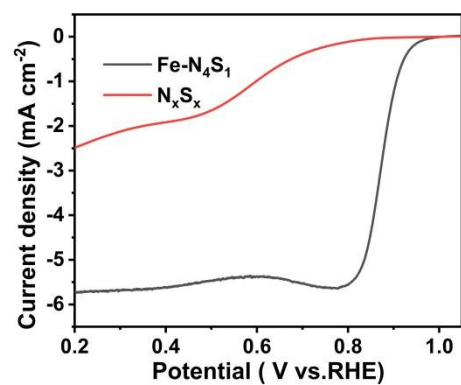


Figure S16. ORR performances in 0.1 M KOH. LSV curves of Fe-N₄S₁ and N_xS_x.

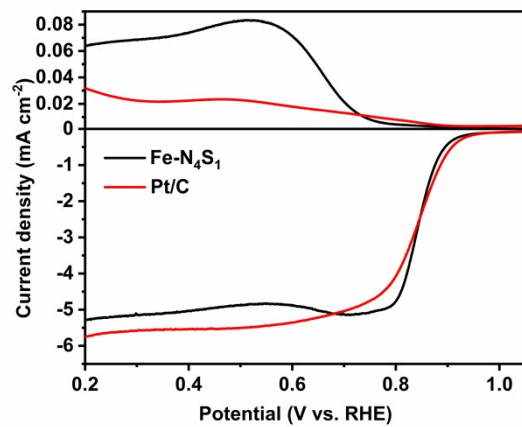


Figure S17. RRDE polarization curves of Fe-N₄S₁ and Pt/C at 1600 rpm with a scan rate of 10 mV s⁻¹.

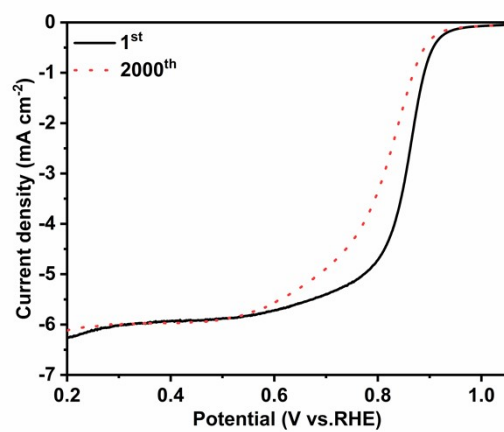


Figure S18. ORR polarization curves before and after 2000 potential cycles for Pt/C.

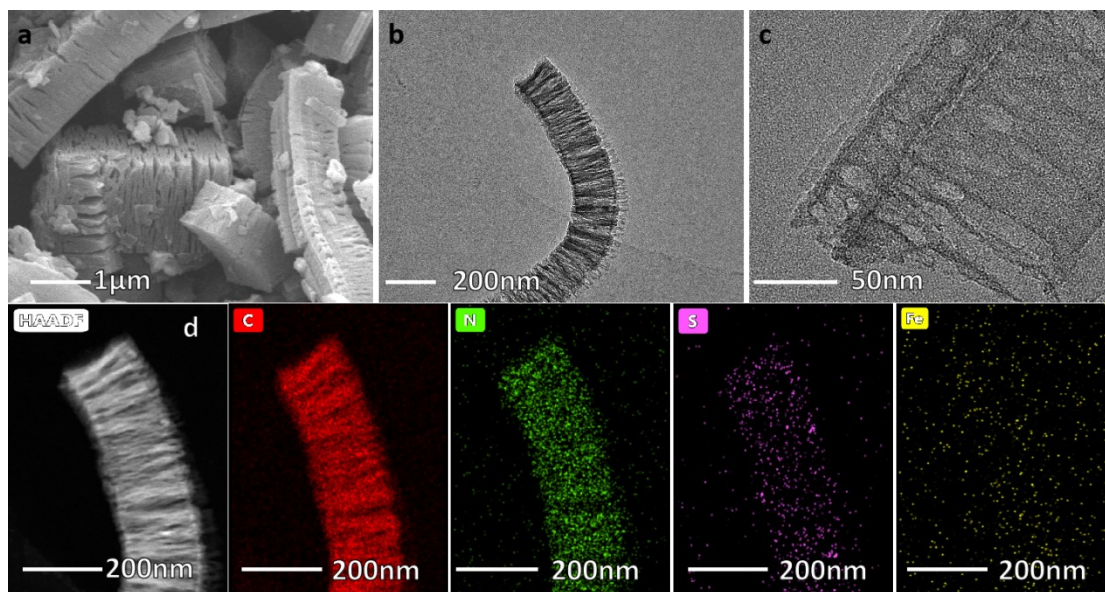


Figure S19 Morphological characterization of Fe-N₄S₁ samples after stabilization. (a) SEM and (b, c) TEM images of Fe-N₄S₁. (d) HAADF-STEM and the elemental mapping of C, N, S and Fe.

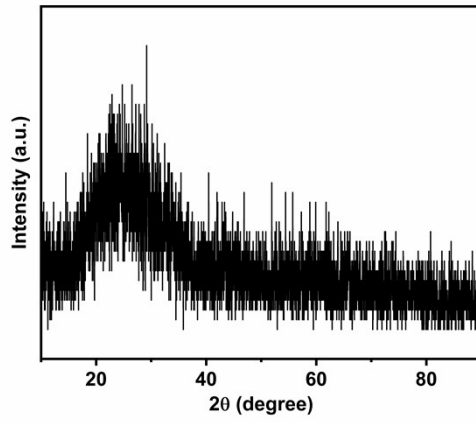


Figure S20. XRD characterization of Fe-N₄S₁ samples after stabilization.

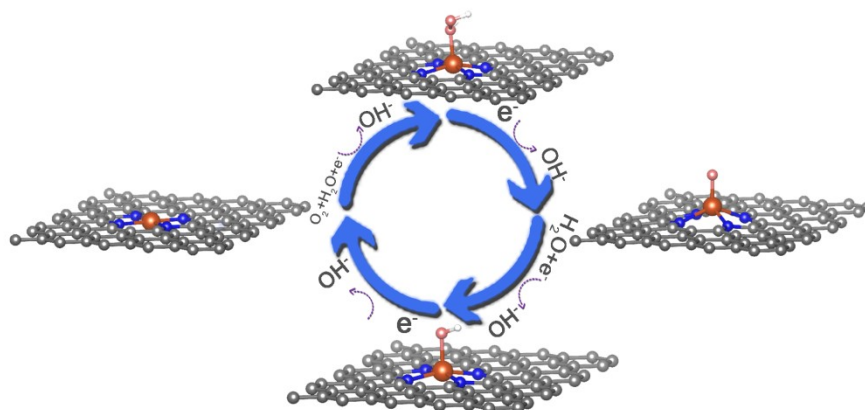


Figure S21. Reaction scheme with intermediates in the ORR process on Fe-N₄.

Table S1. ICP of S and Fe elements in the sample.

Samples	Element	Quality Score (%)
Fe-D	Fe	0.0244
Fe-S	Fe	2.8805
Fe-N_x	Fe	0.0143
Fe-N₄S₁	Fe	1.4495
Fe-S	S	4.4359
Fe-N₄S₁	S	0.5272

Table S2. Structural parameters extracted from EXAFS data fitting of ($S_0^2 = 1$)

	Bond type	N	R (\AA^2)	$\sigma^2(\text{\AA}^2)$	R-factor
Fe-N₄S₁	Fe-N	4	1.96	0.00505	0.014
	Fe-S	1	2.28	0.00113	

Table S3. ORR performance comparison in 0.1 M KOH.

Catalyst	E_{onset}(V vs.RHE)	E_{1/2}(V vs.RHE)	References
Fe-N ₄ S ₁	0.96	0.88	This work
Fe-D	0.86	0.79	This work
Fe-S	0.92	0.84	This work
Fe-N	0.88	0.81	This work
PCN-226(Co)	0.83 V	0.75 V	[6]
Co-N-C (A)	--	0.89 V	[7]
CoSe ₂ @NC	0.904 V	0.83 V	[8]
CoFe/S-N-C	--	0.855 V	[9]
FePc&rGO	0.98 V	0.89 V	[10]
Co-SAC/NC	1.019 V	0.884 V	[11]
Fe/OES	1.0 V	0.85 V	[12]
NiFe@C@Co CNFs	0.94 V	0.87 V	[13]
CoN ₃ C ₁	0.904 V	0.824 V	[14]
Ni-N ₄	0.97 V	0.86 V	[15]
CuZn/NC	0.982 V	0.884 V	[16]
N-CN ₂ P	0.96 V	0.85 V	[17]
Fe ²⁺ @NCS-A	0.94 V	0.79 V	[18]
Co/MnO@NC	0.96 V	0.83 V	[19]
NPCS-900	0.99 V	0.87 V	[20]
Fe-N/GNs	0.903 V	0.837 V	[21]
Cu SAs/NC-900	--	0.87 V	[22]
Co-pyridinic N-C	0.99 V	0.87 V	[23]
PSTA-Co-1000	--	0.878 V	[24]

Table S4. Calculated ΔG for $4e^-$ ORR pathway on Fe-N₄ and Fe-N₄S₁ at U = 0 V vs.

U = 0 V	O ₂ (eV)	OOH*(eV)	O* (eV)	OH* (eV)	OH ⁻ (eV)
Fe-N ₄ S ₁	4.92	4.327813	3.2137	1.133447	0
Fe-N ₄	4.92	3.687101	1.453058	0.515673	0

Table S5. Calculated ΔG for $4e^-$ ORR pathway on Fe-N₄ and Fe-N₄S₁ at U = 1.23 V.

U = 1.23 V	O ₂ (eV)	OOH*(eV)	O* (eV)	OH* (eV)	OH ⁻ (eV)
Fe-N ₄ S ₁	0	-0.0029	-1.00694	-0.71433	0
Fe-N ₄	0	0.637813	0.7537	-0.09655	0

References

- [1] G. Kresse, J. Furthmüller, *Phys. Rev.*, 1996, **54**, 11169.
- [2] T. Björkman, *Comput Phys Commun.*, 2011, **182**, 1183-1186.
- [3] J.P. Perdew, K. Burke, M. Ernzerhof, *Phys. Rev. Lett.*, 1996, **77**, 3865.
- [4] L. Schimka, J. Harl, A. Stroppa, A. Grüneis, M. Marsman, F. Mittendorfer, G. Kresse, *Nat. Mater.*, 2010, **9**, 741-744.
- [5] H.J. Monkhorst, J.D. Pack, *Phys. Rev. B*, 1976, **13**, 5188.
- [6] M.O. Cichocka, Z. Liang, D. Feng, S. Back, S. Siahrostami, X. Wang, L. Samperisi, Y. Sun, H. Xu, N. Hedin, *J. Am. Chem. Soc.*, 2020, **142**, 15386-15395.
- [7] J. Gao, Y. Hu, Y. Wang, X. Lin, K. Hu, X. Lin, G. Xie, X. Liu, K.M. Reddy, Q. Yuan, *Small*, 2021, **17**, 2104684.
- [8] K. Ding, J. Hu, J. Luo, W. Jin, L. Zhao, L. Zheng, W. Yan, B. Weng, H. Hou, X. Ji, *Nano Energy*, 2022, **91**, 106675.
- [9] G. Li, Y. Tang, T. Fu, Y. Xiang, Z. Xiong, Y. Si, C. Guo, Z. Jiang, *Chem. Eng. J.*, 2022, **429**, 132174.
- [10] Z.-y. Mei, S. Cai, G. Zhao, Q. Jing, X. Sheng, J. Jiang, H. Guo, *Energy Stor. Mater.*, 2022, **50**, 12-20.
- [11] P. Rao, J. Luo, D. Wu, J. Li, Q. Chen, P. Deng, Y. Shen, X. Tian, *Energy Environ. Sci.*, 2022.
- [12] C.C. Hou, L. Zou, L. Sun, K. Zhang, Z. Liu, Y. Li, C. Li, R. Zou, J. Yu, Q. Xu, *Angew. Chem. Int. Ed.*, 2020, **132**, 7454-7459.
- [13] X. Chen, J. Pu, X. Hu, Y. Yao, Y. Dou, J. Jiang, W. Zhang, *Small*, 2022, **18**, 2200578.
- [14] X. Hai, X. Zhao, N. Guo, C. Yao, C. Chen, W. Liu, Y. Du, H. Yan, J. Li, Z. Chen, *ACS Catal.*, 2020, **10**, 5862-5870.
- [15] Z. Cai, P. Du, W. Liang, H. Zhang, P. Wu, C. Cai, Z. Yan, *J. Mater. Chem. A*, 2020, **8**, 15012-15022.
- [16] D. Qi, Y. Liu, M. Hu, X. Peng, Y. Qiu, S. Zhang, W. Liu, H. Li, G. Hu, L. Zhuo, *Small*, 2020, **16**, 2004855.
- [17] L. Zong, W. Wu, S. Liu, H. Yin, Y. Chen, C. Liu, K. Fan, X. Zhao, X. Chen, F. Wang, *Energy Stor. Mater.*, 2020, **27**, 514-521.
- [18] J. Feng, R. Cai, E. Magliocca, H. Luo, L. Higgins, G.L.F. Romario, X. Liang, A. Pedersen, Z. Xu, Z. Guo, *Adv. Funct. Mater.*, 2021, **31**, 2102974.
- [19] Y. Niu, X. Teng, S. Gong, X. Liu, M. Xu, Z. Chen, *Energy Stor. Mater.*, 2021, **43**, 42-52.
- [20] G. Ren, S. Chen, J. Zhang, N. Zhang, C. Jiao, H. Qiu, C. Liu, H.-L. Wang, *J. Mater. Chem. A*, 2021, **9**, 5751-5758.
- [21] D. Liu, J.C. Li, S. Ding, Z. Lyu, S. Feng, H. Tian, C. Huyan, M. Xu, T. Li, D. Du, *Small Methods*, 2020, **4**, 1900827.
- [22] S. Ma, Z. Han, K. Leng, X. Liu, Y. Wang, Y. Qu, J. Bai, *Small*, 2020, **16**, 2001384.
- [23] Y. Ha, B. Fei, X. Yan, H. Xu, Z. Chen, L. Shi, M. Fu, W. Xu, R. Wu, *Adv. Energy Mater.*, 2020, **10**, 2002592.

[24] X. Wei, D. Zheng, M. Zhao, H. Chen, X. Fan, B. Gao, L. Gu, Y. Guo, J. Qin, J. Wei, *Angew. Chem. Int. Ed.*, 2020, **132**, 14747-14754.